IEEE Access
Multidisciplinary ⋮ Rapid Review ⋮ Open Access Journal

Received February 16, 2021, accepted March 23, 2021, date of publication April 30, 2021, date of current version May 10, 2021.

Digital Object Identifier 10.1109/ACCESS.2021.3076931

A Time-Domain Numerical Method for Multi-Conductor Coaxial Lines Using the Exact Retarded Potential Integral Equations

SHUJI KITORA, SOUMA JINNO, HIROSHI TOKI, AND MASAYUKI ABE, (Member, IEEE)
Graduate School of Engineering Science, Osaka University, Toyonaka 560-8531, Japan

Corresponding author: Shuji Kitora (u760406f@alumni.osaka-u.ac.jp)

This work was supported in part by the Grant-in-Aid for the Japan Society for the Promotion of Science (JSPS) Fellows under Grant 19J14259, and in part by the Grant-in-Aid for Scientific Research under Grant 19H05789.

ABSTRACT We present a time-domain numerical method for calculating the current propagating through coaxial lines including the radiation effect. In previous studies of transmission lines using the retarded potential integral equations (RPIE), the so-called thin-wire approximation to the RPIE has been mainly used. However, the thin-wire approximation has the problem that the unphysical oscillation occurs when the spatial mesh size is smaller than the radius, even for one-conductor line. In addition, the application of the thin-wire approximation in multi-conductor coaxial lines causes a problem in the formulation. We solve these problems by developing a numerical method using the exact RPIE. We perform numerical calculations in the time-domain for two-conductor coaxial lines and obtain numerical solutions even for the very small common-mode current that causes radiation emission.

INDEX TERMS Coaxial lines, time-domain, common-mode, retarded potential, integral equation.

I. INTRODUCTION

It has been pointed out that the common-mode current[1] can generate a large amount of electromagnetic radiation emission with a value much smaller than the normal-mode (differential-mode) current in the two wires [5], [6]. Therefore, it is important to accurately calculate even a small value of common-mode current in the electromagnetic interference (EMI) analysis. Common-mode currents are generated by structural asymmetries in electric circuits and transmission lines [7]. Hence, in transmission lines such as coaxial lines or parallel lines with different radii, common-mode currents are excited, which could become a source of electromagnetic radiation.

However, the classical transmission line theory in terms of the Heaviside telegraph equations can handle only the normal-mode current and cannot treat the common-mode current of two conductors [1], [6]. Hence, in order to deal with the common-mode current and the electromagnetic radiation, we need to use an extended transmission line theory that includes the retarded potential integral equations (RPIE) [1]–[3], [8]–[10].

In such approaches, the thin-wire approximation is commonly used, which assumes that the current flows in the center of the axis for simplicity [1]–[3], [8], [10]. Using the thin-wire approximation for two parallel conductor lines with the same radii, the normal-mode and common-mode decouple each other. In this case, the numerical results unchanged by varying the mesh size within the region larger than the radii of the two lines [10]. On the other hand, when the radii are different, the normal-mode and common-mode couple, and even if the input is applied only to the normal mode, a small common-mode current is excited due to structural asymmetry. In this case, the numerical results changed by varying the mesh size within the region larger than the radii [10]. By going further to smaller mesh size, we encountered numerical results with an unphysical oscillating pattern [10]. It is a difficult problem to calculate the small common-mode current excited by asymmetry, and we have to reconsider the formulation performed under the thin-wire approximation from the beginning to overcome the difficulty.

The associate editor coordinating the review of this manuscript and approving it for publication was Flavia Grassi.

[1]We note that the term "antenna-mode" is used for common-mode in two-conductor lines in Ref [1]–[3]. In the case of three-conductor lines, the term "common-mode" is also used for the mutual mode among the three lines [4], but it is different from the two-conductor common-mode current discussed in this paper.

The aforementioned unphysical oscillating pattern are known to be the problem arising from the ill-posedness of the integral equation using the thin-wire approximation [11], [12]. Fikioris *et al.* gave a clear insight into overcoming this problem in their study of a very simple electrostatic problem in one-conductor line [13]. They demonstrated that the unphysical oscillation occurs in the charge distribution at both ends of the line even for the electrostatic case when the spatial mesh size is smaller than the radius. As the way out, they treated the integral equation rigorously without any approximation for the one conductor case, and showed that charge distributions can be calculated without the unphysical oscillation.

This finding urged us to treat a two-conductor transmission line system rigorously without any approximation to the RPIE. Here, we want to take two-conductor lines with different radii for the study of the coupling problem between normal-mode and common-mode. Out of various possibilities, only two-conductor coaxial lines hold the axial symmetry, where the formulation is transparent. Hence, we take two-conductor coaxial lines in the present study in order to discuss the convergence problem in the common-mode current without much computational complexity. We note that the use of the thin-wire approximation for two-conductor coaxial lines is conceptually problematic because the centers of the two lines are in the same place.

Most of the analysis of the common-mode current has been performed in the frequency domain [1]–[3]. In the frequency domain, however, it is difficult to identify the source of the coupling of the common-mode with the normal-mode. On the other hand, by analyzing the system in the time-domain, it is possible to understand the mechanism of electromagnetic noise generation such as where and how the normal- and common-mode currents are coupled. There is a study of the numerical method in the time-domain using the exact RPIE in a single conductor [14]. In the numerical method, however, they introduced an additional approximation in the treatment of the delay term. We develop a numerical method that does not apply any additional approximations for the calculation of the delay term, except for discretizing the exact RPIE using the collocation method [15].

In this paper, we study a numerical method of multi-conductor coaxial lines in the time domain using the exact RPIE. We numerically calculate the normal- and common-mode currents for two-conductor coaxial lines.

This paper is organized as follows. In section 2, we formulate coupled integral and partial-differential equations for multi-conductor coaxial lines derived from the Maxwell equations, and give a numerical method for the derived equations using the collocation method [15] and finite difference time-domain (FDTD) method. In section 3, we show the numerical results for one-conductor line and two-conductor coaxial lines in the time-domain. In section 4, we present the conclusions of this study. We write Appendix for the details of the numerical method.

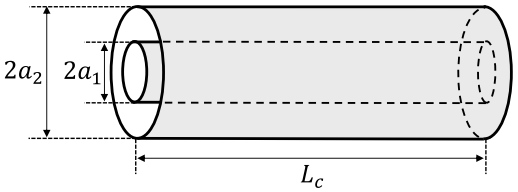

FIGURE 1. Two-conductor coaxial lines with the diameters $2a_1$ and $2a_2$ and the length of L_c. The internal conductor is hollow and thin, and not connected to the outer thin conductor in both ends.

II. FORMULATION AND NUMERICAL METHODS

A. COUPLED INTEGRAL AND PARTIAL-DIFFERENTIAL EQUATIONS FOR COAXIAL LINES

We consider multi-conductor coaxial lines of N_c conductors, where the conductors are assumed to be perfect conductors. We show the case of $N_c = 2$ in Fig. 1. The length of the conductor is L_c and the radius of each line is a_k $(k = 1, \ldots, N_c)$. We start with the retarded potential integral equations (RPIE) derived from the Maxwell equations in the Lorenz gauge as

$$U(\mathbf{r}, t) = \frac{1}{4\pi\varepsilon}\int_{V'} \frac{\rho(\mathbf{r}', t - |\mathbf{r} - \mathbf{r}'|/c)}{|\mathbf{r} - \mathbf{r}'|} d\mathbf{r}' , \tag{1}$$

$$\mathbf{A}(\mathbf{r}, t) = \frac{\mu}{4\pi}\int_{V'} \frac{\mathbf{J}(\mathbf{r}', t - |\mathbf{r} - \mathbf{r}'|/c)}{|\mathbf{r} - \mathbf{r}'|} d\mathbf{r}' . \tag{2}$$

Here, ρ is the charge density $\mathrm{C/m^3}$, $\mathbf{J}$ is the current density vector $\mathrm{A/m^2}$. ε and μ are permittivity and permeability in vacuum, respectively. We use the primed coordinates for source locations, while the unprimed ones for observer locations. Here, $|\mathbf{r} - \mathbf{r}'|/c$ is the time for the signal to propagate from the source at $\mathbf{r}'$ to the potential at $\mathbf{r}$ with the speed of light c. Hence, this term $|\mathbf{r} - \mathbf{r}'|/c$ is named as delay term.

We take the cylindrical coordinate system (r, ϕ, x) and assume that the current flows only in the x-direction due to the axial symmetry of the coaxial lines. The vector potential has only the x component, and the x component A_x of the vector potential is simply written as A, and the x component J_x of the current density vector as J. Furthermore, since the coaxial lines has axial symmetry, we set $\phi = 0$ for the scalar and vector potential without loss of generality. The scalar and vector potentials on the surface of the k-th conductor are expressed as U_k and A_k, respectively. Assuming that the conductor thickness is infinitely thin, the charge density and current density are given as follows.

$$\rho(r', \phi', x', t') = \begin{cases} \sum_{l=1}^{N_c} \tilde{\rho}_l(x', t')\delta(r' - a_l) & 0 \le x' \le L_c \\ 0 & \text{otherwise} \end{cases} \tag{3}$$

$$J(r', \phi', x', t') = \begin{cases} \sum_{l=1}^{N_c} \tilde{J}_l(x', t')\delta(r' - a_l) & 0 \le x' \le L_c \\ 0 & \text{otherwise} \end{cases} \tag{4}$$

Here, the units of $\tilde{\rho}_l$, and $\tilde{J}_l$ are changed from ρ and J as $\mathrm{C/m^2}$ and $\mathrm{A/m}$, respectively. The charge and current do not have ϕ' dependence due to the axial symmetry.

Substituting (3) into (1) and (4) into (2) gives the following integral equations.

$$U_k(x,t) = \sum_{l=1}^{N_c} \frac{1}{4\pi\varepsilon} \int_0^{L_c} \int_{-\pi}^{\pi} \times \frac{\tilde{\rho}_l(x', t - R_{kl}(x-x',\phi')/c)}{R_{kl}(x-x',\phi')} a_l d\phi' dx' \,, \quad (5)$$

$$A_k(x,t) = \sum_{l=1}^{N_c} \frac{\mu}{4\pi} \int_0^{L_c} \int_{-\pi}^{\pi} \times \frac{\tilde{J}_l(x', t - R_{kl}(x-x',\phi')/c)}{R_{kl}(x-x',\phi')} a_l d\phi' dx' \,, \quad (6)$$

where

$$R_{kl}(x,\phi) = \sqrt{x^2 + a_k^2 + a_l^2 - 2a_k a_l \cos\phi} \,. \quad (7)$$

Here, $R_{kl}(x,\phi)$ is the distance between the position of the potential and the source. Due to the axial symmetry, we can write line charge density ρ_l in unit of C/m, and the current I_l in unit of A are written as

$$\rho_l(x,t) = 2\pi a_l \tilde{\rho}_l(x,t) \quad (8)$$

$$I_l(x,t) = 2\pi a_l \tilde{J}_l(x,t) \quad (9)$$

We can then arrive at the following equations.

$$U_k(x,t) = \sum_{l=1}^{N_c} \frac{1}{8\pi^2\varepsilon} \int_0^{L_c} \int_{-\pi}^{\pi} \times \frac{\rho_l(x', t - R_{kl}(x-x',\phi')/c)}{R_{kl}(x-x',\phi')} d\phi' dx', \quad (10)$$

$$A_k(x,t) = \sum_{l=1}^{N_c} \frac{\mu}{8\pi^2} \int_0^{L_c} \int_{-\pi}^{\pi} \times \frac{I_l(x', t - R_{kl}(x-x',\phi')/c)}{R_{kl}(x-x',\phi')} d\phi' dx' \,. \quad (11)$$

There are charge conservation equations to be satisfied between the line charge density and current for each line $k = 1, \ldots, N_c$.

$$\frac{\partial \rho_k(x,t)}{\partial t} + \frac{\partial I_k(x,t)}{\partial x} = 0 \,. \quad (12)$$

Additionally, we take the relation of the scalar and vector potentials of each line for a perfect conductor.

$$\frac{\partial U_k(x,t)}{\partial x} + \frac{\partial A_k(x,t)}{\partial t} = 0 \,. \quad (13)$$

With these four fundamental equations (10), (11), (12), (13), we can treat the propagation of signals in coaxial lines, taking into account the radiation effects.

We take simple boundary conditions as given for each conductor k as follows.

$$I_k(0,t) = I_k^B(t) \,,$$
$$I_k(L_c,t) = 0 \,. \quad (14)$$

where $I_k^B(t)$ is a given function and is used as input to each line from the left end. Also, as the initial condition, all quantities are set to zero for $t \le 0$.

B. NUMERICAL METHODS FOR DERIVED EQUATIONS

We introduce here the collocation method and the FDTD method for numerical calculations. We divide a line of length L_c into N_x small areas with a mesh size $\Delta x = L_c/N_x$. The time step Δt is related with $\Delta x = \alpha c \Delta t$ with a parameter α, where c is the speed of light. The number of time steps is expressed as N_t.

Since we take the FDTD method for discretization of the partial differential equations, we shift the mesh points for the current and vector potential from those of the charge and scalar potential by a half-integer as

$$x_i^A = (i + 1/2)\Delta x, \quad (i = 0, \ldots, N_x - 1) \,, \quad (15)$$
$$t_n^A = (n+1)\Delta t, \quad (n = 0, \ldots, N_t - 1) \,. \quad (16)$$

We write the vector potential and current at the mesh points as

$$A_k^{n,i} = A_k(x_i^A, t_n^A) \,, \quad (17)$$
$$I_k^{n,i} = I_k(x_i^A, t_n^A) \,. \quad (18)$$

Similarly, for the charge and scalar potential, we write

$$x_i^U = (i+1)\Delta x, \quad (i = 0, \ldots, N_x - 2) \,, \quad (19)$$
$$t_n^U = (n + 3/2)\Delta t, \quad (n = 0, \ldots, N_t - 2) \,, \quad (20)$$

and

$$U_k^{n,i} = U_k(x_i^U, t_n^U) \,, \quad (21)$$
$$\rho_k^{n,i} = \rho_k(x_i^U, t_n^U) \,. \quad (22)$$

For illustration, we show the collocation points of the scalar potential $U_k^{n,i}$ and the vector potential $A_k^{n,i}$ together with the current $I_k^{n,i}$ and charge $\rho_k^{n,i}$ in the space-time plane in Fig. 2.

We discretize the integral equation (11) for the current and vector potential using the collocation method. We expand the current using the pulse function and the value at each mesh point.

$$I_l(x,t) = \sum_{j=0}^{N_x-1} \sum_{m=0}^{N_t-1} I_l^{m,j} f_j^I(x) g_m^I(t) \,, \quad (23)$$

where the space pulse function is written as

$$f_j^I(x) = \begin{cases} 1 & j\Delta x \le x < (j+1)\Delta x \,, \\ 0 & \text{otherwise} \,. \end{cases} \quad (24)$$

and the time pulse function is

$$g_m^I(t) = \begin{cases} 1 & m\Delta t < t \le (m+1)\Delta t \,, \\ 0 & \text{otherwise} \,. \end{cases} \quad (25)$$

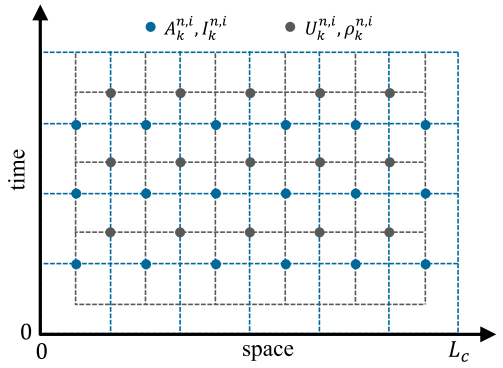

FIGURE 2. Collocation points of the scalar potential $U_k^{n,i}$ and the vector potential $A_k^{n,i}$ together with the current $I_k^{n,i}$ and charge $\rho_k^{n,i}$ are shown in the space-time plane. The collocation points of $U_k^{n,i}$ and $\rho_k^{n,i}$ are denoted by the black points at the same positions, while the collocation points of $A_k^{n,i}$ and $I_k^{n,i}$ are denoted by the blue points, which are shifted by a half-integer from those of $U_k^{n,i}$ and $\rho_k^{n,i}$.

Hence, we can write the vector potential (11) at the collocation point (x_i^A, t_n^A) as

$$A_k^{n,i} = \sum_{l=1}^{N_c} \frac{\mu}{8\pi^2} \int_0^{L_c} \int_{-\pi}^{\pi} d\phi' dx' \times \frac{I_l(x', t_n^A - R_{kl}(x_i^A - x', \phi')/c)}{R_{kl}(x_i^A - x', \phi')} \tag{26}$$

Inserting (23), we get

$$A_k^{n,i} = \sum_{l=1}^{N_c} \sum_{j=0}^{N_x-1} \sum_{m=0}^{N_t-1} L_{k,l}^{n,m,i,j} I_l^{m,j} , \tag{27}$$

where

$$L_{k,l}^{n,m,i,j} = \frac{\mu}{8\pi^2} \int_0^{L_c} \int_{-\pi}^{\pi} d\phi' dx' \times \frac{f_j^I(x') g_m^I(t_n^A - R_{kl}(x_i^A - x', \phi')/c)}{R_{kl}(x_i^A - x', \phi')} . \tag{28}$$

We use equation (27) to calculate the unknown currents from the known vector potentials and currents. We describe this detail in the Appendix A.

Using (24), we can write the local delay inductance as

$$L_{k,l}^{n,m,i,j} = \frac{\mu}{8\pi^2} \int_{j\Delta x}^{(j+1)\Delta x} \int_{-\pi}^{\pi} d\phi' dx' \times \frac{g_m^I(t_n^A - R_{kl}(x_i^A - x', \phi')/c)}{R_{kl}(x_i^A - x', \phi')} . \tag{29}$$

Here, $L_{k,l}^{n,m,i,j}$ is symmetric for i and j, and depend only on the difference $|i-j|$. As for the n and m, the local delay inductance depends only on the difference $n-m$. Here, we introduce the local delay impedance as,

$$Z_{k,l}^{n,i} = \zeta \int_{x_i^-}^{x_i^+} \int_{-\pi}^{\pi} \frac{g_n(R_{kl}(x,\phi)/c)}{R_{kl}(x,\phi)} d\phi dx , \tag{30}$$

with $\zeta = \frac{1}{8\pi^2} Z_0$, where $Z_0 = \sqrt{\mu/\varepsilon}$ is the impedance of the vacuum. Hence, $Z_{k,l}^{n,i}$ has the dimension of the resistance. For the upper and lower bound of the integral we use $x_i^{\pm} = (i \pm 1/2)\Delta x$, and the pulse function as

$$g_n(t) = \begin{cases} 1 & n\Delta t \le t < (n+1)\Delta t , \\ 0 & \text{otherwise} . \end{cases} \tag{31}$$

We can write the local delay inductance $L_{k,l}^{n,m,i,j}$ (29) in terms of the local delay impedance $Z_{k,l}^{n,i}$ (30) as

$$L_{k,l}^{n,m,i,j} = \frac{1}{c} Z_{k,l}^{n-m,|i-j|} \tag{32}$$

Similarly, we discretize the integral equation (10) for the line charge density and scalar potential using the collocation method. We expand the line charge density using the pulse function as

$$\rho_l(x,t) = \sum_{j=0}^{N_x-2} \sum_{m=0}^{N_t-2} \rho_l^{m,j} f_j^{\rho}(x) g_m^{\rho}(t) . \tag{33}$$

Here, the pulse function in the x direction is

$$f_j^{\rho}(x) = \begin{cases} 1 & (j+1/2)\Delta x \le x < (j+3/2)\Delta x , \\ 0 & \text{otherwise} . \end{cases} \tag{34}$$

and the time direction is

$$g_m^{\rho}(t) = \begin{cases} 1 & (m+1/2)\Delta t < t \le (m+3/2)\Delta t , \\ 0 & \text{otherwise} . \end{cases} \tag{35}$$

From (10), we write the scalar potential $U_k^{n,i}$ at the collocation point (x_i^U, t_n^U) as

$$U_k^{n,i} = \sum_{l=1}^{N_c} \sum_{j=0}^{N_x-2} \sum_{m=0}^{N_t-2} P_{k,l}^{n,m,i,j} \rho_l^{m,j} , \tag{36}$$

where

$$P_{k,l}^{n,m,i,j} = \frac{1}{8\pi^2\varepsilon} \int_0^{L_c} \int_{-\pi}^{\pi} d\phi' dx' \times \frac{f_j^{\rho}(x') g_m^{\rho}(t_n^U - R_{kl}(x_i^U - x', \phi')/c)}{R_{kl}(x_i^U - x', \phi')} . \tag{37}$$

This coefficient $P_{k,l}^{n,m,i,j}$ can be written in terms of the local delay impedance $Z_{k,l}^{n,i}$ (30) as

$$P_{k,l}^{n,m,i,j} = c Z_{k,l}^{n-m,|i-j|} \tag{38}$$

We calculate $Z_{k,l}^{n,i}$ by numerically integrating the equation (30). Since the integrand of (30) diverges at $k = l, i = 0, n = 0$ and $\phi' = 0, x' = 0$, we need to be careful about the treatment of this singularity in the numerical

integration. If this singularity is avoided in the nodes of the numerical integration, the approximate value of integral can be obtained, but the convergence of the numerical integration is slow. Hence, we divide the region of integration and perform singular integration analytically. We write the details of this method in the Appendix B.

In mutual terms other than the above self term, the integrand does not diverge. On the other hand, due to the basis function (31) in the numerator, the integrand may be a discontinuous function, in which case the numerical integration converges slowly. Therefore, the numerical integration is performed after finding the domain of integration where the integrand is not zero. Since it is an important point in the treatment of the local delay impedance, we provide the detail in the Appendix C.

We discretize the partial differential equation (12) using the FDTD method.

$$\frac{\rho_k^{n,i} - \rho_k^{n-1,i}}{\Delta t} + \frac{I_k^{n,i+1} - I_k^{n,i}}{\Delta x} = 0 \tag{39}$$

We rewrite this equation to express $\rho_k^{n,i}$ in terms of known quantities.

$$\rho_k^{n,i} = \rho_k^{n-1,i} - \frac{\Delta t}{\Delta x}(I_k^{n,i+1} - I_k^{n,i}) \tag{40}$$

Similarly, we discretize the partial differential equation (13) using the FDTD method.

$$\frac{A_k^{n,i} - A_k^{n-1,i}}{\Delta t} + \frac{U_k^{n-1,i} - U_k^{n-1,i-1}}{\Delta x} = 0 \tag{41}$$

We rewrite this equation to express $A_k^{n,i}$ in terms of known quantities.

$$A_k^{n,i} = A_k^{n-1,i} - \frac{\Delta t}{\Delta x}(U_k^{n-1,i} - U_k^{n-1,i-1}) \tag{42}$$

As for the boundary condition (14), we take

$$I_k^{n,0} = I_k^B(t_n^A)\,, \tag{43}$$

$$I_k^{n,N_x-1} = 0\,. \tag{44}$$

From the initial condition, we set all quantities are 0 for $n \leq 0$. For $n \geq 1$, using (42) we calculate $A_k^{n,i}$, and use (59) to find $I_k^{n,i}$ at the places other than the boundary. Then, using (40) to find $\rho_k^{n,i}$, and (36) to find $U_k^{n,i}$. Increasing time steps one by one, the values of the later time are repeatedly obtained. We show the flowchart of numerical calculations in Fig. 3.

III. NUMERICAL RESULTS

In this section, we obtain numerical results in one- and two-line systems using numerical methods described in the previous section. First, we compare the exact case and the case with the thin-wire approximation in the calculation of one conductor line. For the numerical calculation of the thin-wire approximation in the time-domain, we use the method described by Kitora *et al.* [10]. We shall show next the numerical results for the normal-mode and common-mode currents in the two-conductor coaxial lines.

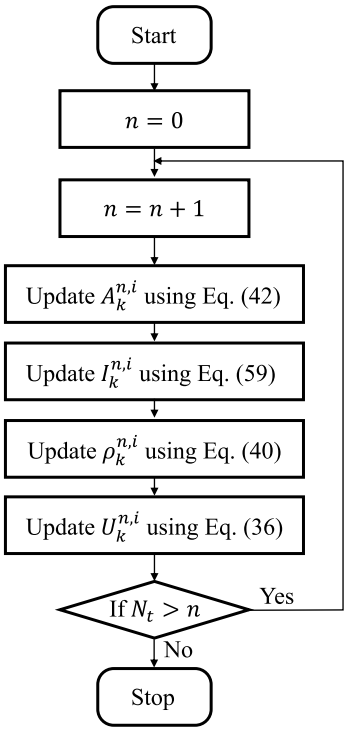

FIGURE 3. The flowchart of numerical calculations.

A. NUMERICAL RESULTS FOR A SINGLE CONDUCTOR

Here, we compare the thin-wire approximation and the exact expression in one conductor. It is important to understand that the thin-wire approximation gives an oscillatory behavior due to the ill-posed problem even in the electrostatic case of one conductor. In a recent paper, a comparison of thin-wire approximation and exact treatment in the electrostatic case is discussed by Fikioris *et al.* [13]. They consider the charge density distribution in an equipotential line occupying the interval from $-L$ to L. It is known that the solution behaves like $1/\sqrt{L^2 - x^2}$ around $x = \pm L$ [13], [16]. While this behavior can be calculated using the exact representation, the thin-wire approximation causes unphysical oscillations at the boundary when the mesh size Δx is smaller than the radius due to the ill-posedness of the integral equation in the thin-wire approximation.

We compare the thin-wire approximation of one conductor line with the exact expression in the time-domain. For completeness, we write a formula of the thin-wire approximation in the expression of the scalar and vector potential for the one conductor case instead of the potentials expressed rigorously in Eqs. (10) and (11).

$$U(x,t) = \frac{1}{4\pi\varepsilon}\int_0^{L_c} \frac{\rho(x', t - |x - x'|/c)}{R(x - x'; a)}dx'\,, \tag{45}$$

$$A(x,t) = \frac{\mu}{4\pi}\int_0^{L_c} \frac{I(x', t - |x - x'|/c)}{R(x - x'; a)}dx'\,, \tag{46}$$

where

$$R(x - x'; a) = \sqrt{(x - x')^2 + a^2}\,. \tag{47}$$

Here, $R(x - x'; a)$ is the distance between the position of the potential and the source. In the thin-wire approximation, the charge and current are assumed to be at the center of the line. The integrand has no singularities, and the analytical solution of the local delayed impedance can be obtained. Note that we used $|x - x'|/c$ instead of $R(x - x'; a)/c$ for the delay term so that the self term of local delay impedance should not be zero when the spatial mesh is smaller than the radius a.

For the numerical calculation, we take the line length L_c is 1 m, and the radius a is 20 mm. We take Δx is 10 mm, which is smaller than the radius, and α is 1. The Gaussian function with an amplitude of 1 A and a standard deviation of 0.4 ns is used as the input current. The numerical results of the line charge density are shown in Fig. 4. As shown in Fig. 4 (a) and (b), it can be seen that there is a large difference between exact and approximate ones at both ends. Similar to the static case, the line charge density shows a sharp increase at both ends in the exact case, while oscillations occur at both ends of the conductor in the thin-wire approximation. This oscillation occurs when the charge density reaches the ends (right end of Fig. 4 (b)). On the other hand, except for both ends, exact and approximate cases have similar results (Fig. 4 (a), (b) and Fig. 4 (c)). These results are similar to the electrostatic case discussed by Fikioris *et al.* [13]. In order to validate the numerical result in the time-domain using the exact RPIE, we compare the result with a numerical solution obtained by solving the same problem in the frequency domain and performing the inverse discrete Fourier transform, and confirm that the same result are obtained.

Therefore, with the exact RPIE, the spatial mesh size can be reduced regardless of the radius because it does not cause unphysical oscillations even when the spatial mesh size is smaller than the radius. This is an important result to be stressed, since the oscillatory behavior in the thin-wire approximation appears near the edges of the line due to the ill-posedness. The behavior of the current is influenced by the oscillatory behavior of the charge distribution.

B. NUMERICAL RESULTS FOR TWO COAXIAL LINES

We perform the numerical calculation of the two-conductor coaxial lines using the exact RPIE. We take the line length L_c is 1 m, and the conductor radius is $a_1 = 10$ mm and $a_2 = 20$ mm. We input the normal-mode current from the left end using the Gaussian function with an amplitude of 1 A and a standard deviation of 0.4 ns. The currents I_1 and I_2 are calculated by the numerical method developed in the previous section, and the normal-mode and common-mode currents are calculated from them using the following formulas [3].

$$I_n = \frac{1}{2}(I_1 - I_2) \tag{48}$$

$$I_c = I_1 + I_2 \tag{49}$$

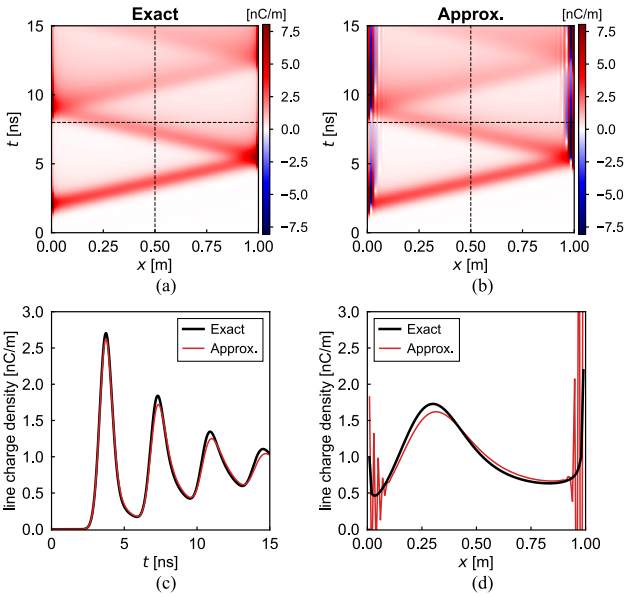

FIGURE 4. Numerical results of line charge density in one conductor line. (a) The two-dimensional plot in exact RPIE case. (b) The two-dimensional plot using thin-wire approximation. (c) Comparison of exact and approximate results at $x = 0.5$ m, which are obtained at the vertical black lines in the two dimensional plots Figs. (a) and (b). (d) Comparison of exact and approximate results at $t = 8$ ns, which are obtained at the horizontal black lines in the two dimensional plots Figs. (a) and (b).

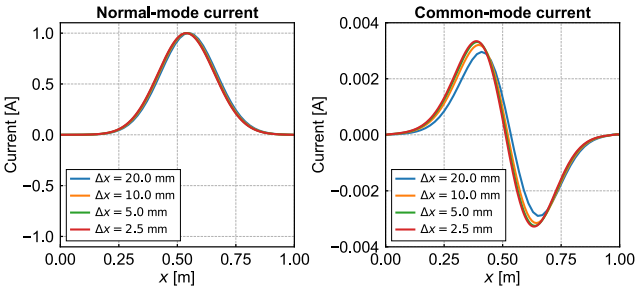

FIGURE 5. Numerical results of the normal-mode current (left) and those of the common-mode current (right) at the time $t = 3.8$ ns as a function of the position x. There are 4 curves in each figure for 4 mesh sizes ranging from 20 mm to 2.5 mm.

First of all, it is important to study the behavior of the common-mode current with respect to the mesh size Δx. The results are shown in Fig. 5. We change the mesh size from $\Delta x = 20$ mm to 2.5 mm, which are smaller than the radius of the conductors. The normal-mode current shown in the left figure is essentially unchanged with the parameter change. The common-mode currents in the right figure tend to converge as the mesh size is reduced. We get satisfactory results on the numerical calculation in terms of convergence without having the unphysical oscillating pattern. Note that in the calculation of two parallel conductor lines with different radii using the thin-wire approximation, the convergence of the common-mode current is not achieved in the region where the mesh size is larger than the radii of the lines, and oscillation patterns are observed as the mesh size becomes smaller than the radii [10].

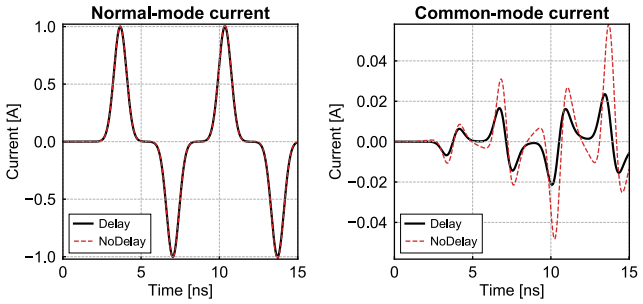

FIGURE 6. Numerical results of the normal-mode current (left) and those of the common-mode current (right) at the middle of the line ($x = 0.5$ m) as functions of time using the mesh size of $\Delta x = 5$ mm. We show two curves in each figure. One is the result of the exact RPIE calculation including the delay term and the other is the calculation without the delay term.

We show the numerical results of the normal and common mode currents at the center of the conductor when using the exact RPIE in the black lines of Fig. 6. We take the mesh size of $\Delta x = 5$ mm, which provides the converged results as shown in Fig. 5. We should note that the magnitude of the excited common-mode current is about a percent of the normal-mode current. It is important to point out the the common-mode current is excited in the coaxial lines due to the asymmetry about the radius of the coaxial lines. For comparison, we show the numerical results for the RPIE formulation by dropping the delay term in Eqs. (10) and (11). The results without the delay term are shown by red dashed-curves in Fig. 6. For the normal-mode current as shown in the left figure in Fig. 6, there is no difference in the results between the case with delay and without delay. On the other hand, for the common-mode currents as shown in the right figure in Fig. 6, the amplitude of the common mode currents with and without delay shows a difference. The magnitudes of the current with the delay term is smaller than those without the delay term, which can be attributed to the fact that the delay term is related to the electromagnetic radiation. These results indicate that in order to accurately calculate the small common-mode currents excited by the coupling between the normal-mode and common-mode currents, it is necessary to perform numerical calculations using an exact RPIE including delay.

Finally, we mention the late-time instability (LTI), which is still a problem in numerical calculations of integral equations in the time-domain [17]. The LTI means that high-frequency oscillation with exponentially increasing amplitude becomes dominant at late times in numerical calculations. We observe the LTI for some values of the parameters α and N_x. The LTI can occurs even when $\alpha \geq 1$, where the Courant-Friedrichs-Lewy (CFL) condition is satisfied. On the other hand, as shown in Fig. 5, when the LTI does not occur, the numerical results tend to converge.

IV. CONCLUSION

We formulated the coupled integral and partial-differential equations describing the signal propagation including the radiation effects in multi-conductor coaxial lines, and gave a numerical method for derived equations using the collocation and FDTD methods. We developed a method to calculate the exact RPIE without using the thin-wire approximation, which has been commonly used in previous studies. Using the thin-wire approximation, even in the time domain, the unphysical oscillation of the line charge density occurs at the edges of conductors when the spatial mesh size is smaller than the radius due to the ill-posed problem. On the other hand, using the exact RPIE, it is possible to compute a sharply rising behavior of the line charge density at the ends of the conductors without oscillations.

In a two-conductor coaxial line system, due to asymmetry of the geometry of the two lines, the common-mode current is excited even if the input is made only for the normal-mode current. Although the amplitude of this common-mode current is much smaller than the amplitude of the normal-mode current, the proposed method using the exact RPIE is able to provide a numerical solution of this common-mode current without the oscillatory behavior. Even if the amplitude of the common-mode current is several orders of magnitude smaller than that of the normal-mode current, the contribution from the common-mode current may be larger in the radiated emission [5], [6].

It would be important to apply the present method for two parallel conductor lines, where the axial symmetry does not hold any more, and the formulation and numerical calculations become cumbersome. Here, we have to describe both the potentials and charge and current as functions of the x position, but also the ϕ directions of the two lines. Even for the multiple-conductor coaxial lines there are many interesting problems as the behaviors of the electromagnetic fields inside and outside of the inner hollow conductor. We can perform the lossy conductors using the Ohm's law instead of the perfect conductor relations. In this study, only the open-end boundary condition were considered, but it is important in applications to consider more general boundary conditions such as connecting lumped-element circuit to the boundary. They are to be performed in near future.

APPENDIX A
NUMERICAL CALCULATION FOR THE CURRENT *I*

We use the equation (27) to calculate the unknown currents $I_k^{n,i} (i = 1, \ldots, N_x - 1)$ from the known vector potentials and currents. We separate the boundary conditions and the known quantities in (27) as

$$\sum_{l=1}^{N_c} \sum_{j=1}^{N_x-2} L_{k,l}^{n,n,i,j} I_l^{n,j} = A_k^{n,i} - \bar{A}_k^{n,i} - \tilde{A}_k^{n,i} . \tag{50}$$

Here, $\bar{A}_k^{n,i}$ is obtained by the boundary conditions,

$$\bar{A}_k^{n,i} = \sum_{l=1}^{N_c} \sum_{j \in \{0, N_x-1\}} L_{k,l}^{n,n,i,j} I_l^{n,j} \tag{51}$$

and $\tilde{A}_k^{n,i}$ is obtained from the past currents,

$$\tilde{A}_k^{n,i} = \sum_{l=1}^{N_c} \sum_{j=0}^{N_x-1} \sum_{m=0}^{n-1} L_{k,l}^{n,m,i,j} I_l^{m,j} . \tag{52}$$

We write the above relation using the matrix representation.

$$\mathbf{I}_l^n = \begin{bmatrix} I_l^{n,1} \\ \vdots \\ I_l^{n,N_x-2} \end{bmatrix}, \quad \mathbf{A}_l^n = \begin{bmatrix} A_l^{n,1} \\ \vdots \\ A_l^{n,N_x-2} \end{bmatrix} \tag{53}$$

$$\bar{\mathbf{A}}_l^n = \begin{bmatrix} \bar{A}_l^{n,1} \\ \vdots \\ \bar{A}_l^{n,N_x-2} \end{bmatrix}, \quad \tilde{\mathbf{A}}_l^n = \begin{bmatrix} \tilde{A}_l^{n,1} \\ \vdots \\ \tilde{A}_l^{n,N_x-2} \end{bmatrix} \tag{54}$$

$$\mathbf{L}_{k,l} = \begin{bmatrix} L_{k,l}^{n,n,1,1} & \cdots & L_{k,l}^{n,n,1,N_x-2} \\ \vdots & \ddots & \vdots \\ L_{k,l}^{n,n,N_x-2,1} & \cdots & L_{k,l}^{n,n,N_x-2,N_x-2} \end{bmatrix} \tag{55}$$

Here, we drop the superscript n and write $\mathbf{L}_{k,l}$, since it does not depend on n.

We further introduce matrices using the above relations as follows

$$\mathbf{I}^n = \begin{bmatrix} \mathbf{I}_1^n \\ \vdots \\ \mathbf{I}_{N_c}^n \end{bmatrix}, \quad \mathbf{A}^n = \begin{bmatrix} \mathbf{A}_1^n \\ \vdots \\ \mathbf{A}_{N_c}^n \end{bmatrix} \tag{56}$$

$$\bar{\mathbf{A}}^n = \begin{bmatrix} \bar{\mathbf{A}}_1^n \\ \vdots \\ \bar{\mathbf{A}}_{N_c}^n \end{bmatrix}, \quad \tilde{\mathbf{A}}^n = \begin{bmatrix} \tilde{\mathbf{A}}_1^n \\ \vdots \\ \tilde{\mathbf{A}}_{N_c}^n \end{bmatrix} \tag{57}$$

$$\mathbf{L} = \begin{bmatrix} \mathbf{L}_{1,1} & \cdots & \mathbf{L}_{1,N_c} \\ \vdots & \ddots & \vdots \\ \mathbf{L}_{N_c,1} & \cdots & \mathbf{L}_{N_c,N_c} \end{bmatrix} \tag{58}$$

Using the above expressions, we can represent the equation (50) as follows

$$\mathbf{L}\mathbf{I}^n = \mathbf{A}^n - \bar{\mathbf{A}}^n - \tilde{\mathbf{A}}^n \tag{59}$$

We obtain $\mathbf{I}^n$ by solving the equation (59).

APPENDIX B
SINGULAR INTEGRAL OF THE LOCAL DELAY IMPEDANCE

We write the detail of the method to treat the singular integral of $Z_{k,l}^{n,i}$ (30). We consider the case $\alpha < 2, c\Delta t \le 2a_k$. When $k = l, i = 0, n = 0$, (30) becomes

$$Z_{k,k}^{0,0} = \zeta \int_{x_0^-}^{x_0^+} \int_{-\pi}^{\pi} \frac{g_0(R_{kk}(x,\phi)/c)}{R_{kk}(x,\phi)} d\phi dx , \tag{60}$$

where

$$R_{kk}(x,\phi) = \sqrt{x^2 + \{2a_k \sin(\phi/2)\}^2} . \tag{61}$$

from (7), and $x_0^{\pm} = \pm\Delta x/2$. We can write g_0 from (31) as follows,

$$g_0(t) = \begin{cases} 1 & 0 \le t < \Delta t , \\ 0 & \text{otherwise} . \end{cases} \tag{62}$$

Since the integrand is an even function, we can write

$$Z_{k,k}^{0,0} = 4\zeta \int_0^{x_0^+} \int_0^{\pi} \frac{g_0(R_{kk}(x,\phi)/c)}{R_{kk}(x,\phi)} d\phi dx , \tag{63}$$

Taking $\phi = 2\psi$,

$$Z_{k,k}^{0,0} = 8\zeta \int_0^{x_0^+} \int_0^{\pi/2} \frac{g_0(r_k(x,\psi)/c)}{r_k(x,\psi)} d\psi dx , \tag{64}$$

where

$$r_k(x,\psi) = \sqrt{x^2 + (2a_k \sin\psi)^2} . \tag{65}$$

The function $r_k(x,\psi)/c$ in (64) is the delay time, and from (62), the integrand is non-zero only for the case $0 \le r_k(x,\psi)/c < \Delta t$. Let $\psi_k(x)$ be a value of ψ such that the delay time is Δt for given x. Thus, from $r_k(x,\psi)/c = \Delta t$, we get

$$\psi_k(x) = \arcsin \frac{\sqrt{(c\Delta t)^2 - x^2}}{2a_k} . \tag{66}$$

We can then write Z in (64) as

$$Z_{k,k}^{0,0} = 8\zeta \int_0^{x_0^+} \int_0^{\psi_k(x)} \frac{1}{r_k(x,\psi)} d\psi dx , \tag{67}$$

where we separate the integral in two terms by using $\psi_k(x_0^+) = \psi_k^+$.

$$Z_{k,k}^{0,0} = 8\zeta [I_0 + I_1] \tag{68}$$

$$I_0 = \int_0^{x_0^+} \int_0^{\psi_k^+} \frac{1}{r_k(x,\psi)} d\psi dx \tag{69}$$

$$I_1 = \int_0^{x_0^+} \int_{\psi_k^+}^{\psi_k(x)} \frac{1}{r_k(x,\psi)} d\psi dx \tag{70}$$

We can then find the singularity only in I_0, and consider the integral I_0.

$$I_0 = \int_0^{\psi_k^+} \int_0^{x_0^+} \frac{1}{\sqrt{x^2 + (2a_k \sin\psi)^2}} dx d\psi \tag{71}$$

$$= \int_0^{\psi_k^+} \left[\log(x + \sqrt{x^2 + (2a_k \sin\psi)^2} \right]_0^{x_0^+} d\psi \tag{72}$$

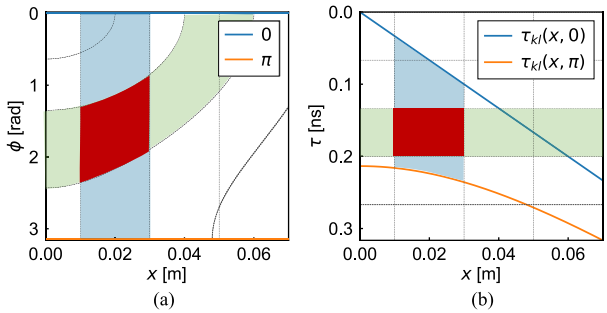

FIGURE 7. An example of the mutual term of local delay impedance. (a) x–ϕ plane. (b) x–τ plane.

We rewrite this as

$$I_0 = I_0^0 + I_0^1 \tag{73}$$

$$I_0^0 = -\int_0^{\psi_k^+} \log(\sin\psi) d\psi \tag{74}$$

$$I_0^1 = \int_0^{\psi_k^+} \log\left(x_0^+ + \sqrt{(x_0^+)^2 + (2a_k \sin\psi)^2}\right) d\psi - \psi_k^+ \log 2a_k \tag{75}$$

The integral I_0^0 with the singularity can be written by using the formula [18],

$$I_0^0 = -\int_0^{\psi_k^+} [\log(\sin\psi) - \log(\psi)] d\psi - \int_0^{\psi_k^+} \log(\psi) d\psi \tag{76}$$

The first non-singular term is calculated numerically, and the second singular term is obtained analytically as follows

$$\int_0^{\psi_k^+} \log(\psi) d\psi = \psi_k^+ \log\psi_k^+ - \psi_k^+ \tag{77}$$

The other non-singular terms (I_0^1, I_1) can be obtained with good accuracy using numerical integration methods such as the Gauss-Legendre quadrature.

APPENDIX C
INTEGRATION REGION OF MUTUAL LOCAL DELAY IMPEDANCE WITH THE DELAY EFFECT

Here, we explain the delay effect on the numerical integration of mutual terms of local delay impedance. Figure 7(a) shows a typical example where the integrand is discontinuous in the calculation of the mutual term of (30). The blue region shows the integration region of (30) in the x–ϕ plane for some i. The green region shows the region where the pulse function g_n is 1 in the numerator of (30) for some n. Therefore, only in the red region where the blue and green regions intersect, the integrand is not zero. On the other hand, it becomes 0 in the other integration region. Hence, the integrand becomes a discontinuous function. Fig. 7(b) shows the integration region in the x–τ plane, where the y-axis in Fig. 7(a) is replaced by the delay time from ϕ. Here, from (30), the delay time $\tau_{kl}(x, \phi)$ is written as

$$\tau_{kl}(x, \phi) = R_{kl}(x, \phi)/c\ . \tag{78}$$

In Fig. 7(b), the blue line shows the value of the delay time for $\phi = 0$, and the orange line shows the value of the delay time for $\phi = \pi$. The blue, green and red regions correspond the regions with the same colors in Fig. 7(a). If numerical integration is performed with the integration region as the blue region, the integrand becomes a discontinuous function, and many nodes are required to obtain the required accuracy. Therefore, by using the red region as the integration region, the integrand becomes a continuous function, and the accuracy of the numerical integration is improved.

REFERENCES

[1] A. Vukicevic, F. Rachidi, M. Rubinstein, and S. V. Tkachenko, "On the evaluation of antenna-mode currents along transmission lines," *IEEE Trans. Electromagn. Compat.*, vol. 48, no. 4, pp. 693–700, Nov. 2006.

[2] D. Liu, Y. Wang, R. W. Kautz, N. Altunyurt, S. Chandra, and J. Fan, "Accurate evaluation of field interactions between cable harness and vehicle body by a multiple scattering method," *IEEE Trans. Electromagn. Compat.*, vol. 59, no. 2, pp. 383–393, Apr. 2017.

[3] H. Toki and K. Sato, "Multiconductor transmission-line theory with electromagnetic radiation," *J. Phys. Soc. Jpn.*, vol. 81, no. 1, Jan. 2012, Art. no. 014201.

[4] H. Toki and K. Sato, "Three conductor transmission line theory and origin of electromagnetic radiation and noise," *J. Phys. Soc. Jpn.*, vol. 78, no. 9, pp. 1–8, 2009.

[5] C. R. Paul and D. R. Bush, "Radiated emissions from common-mode currents," in *Proc. IEEE Int. Symp. Electromagn. Compat.*, no. 4, Aug. 1987, pp. 1–7.

[6] C. R. Paul, "A comparison of the contributions of common-mode and differential-mode currents in radiated emissions," *IEEE Trans. Electromagn. Compat.*, vol. 31, no. 2, pp. 189–193, May 1989.

[7] C. R. Paul, *Introduction to Electromagnetic Compatibility*. Hoboken, NJ, USA: Wiley, 2006.

[8] S. Tkatchenko, F. Rachidi, and M. Ianoz, "Electromagnetic field coupling to a line of finite length: Theory and fast iterative solutions in frequency and time domains," *IEEE Trans. Electromagn. Compat.*, vol. 37, no. 4, pp. 509–518, Nov. 1995.

[9] A. Maffucci, G. Miano, and F. Villone, "An enhanced transmission line model for conducting wires," *IEEE Trans. Electromagn. Compat.*, vol. 46, no. 4, pp. 512–528, Nov. 2004.

[10] S. Kitora, S. Jinno, H. Toki, and M. Abe, "Relation of integro-partial differential equations with delay effect based on the Maxwell equations to the Heaviside and Pocklington equations," *IEEE Trans. Electromagn. Compat.*, early access, Nov. 5, 2020, doi: 10.1109/TEMC.2020.3032788.

[11] R. Bancroft, *Understanding Electromagnetic Scattering Using the Moment Method: A Practical Approach*, vol. 1. Norwood, MA, USA: Artech House, 1996.

[12] P. J. Davies, B. P. Rynne, and B. Zubik-Kowal, "The time domain integral equation for a straight thin-wire antenna with the reduced kernel is not well-posed," *IEEE Trans. Antennas Propag.*, vol. 50, no. 8, pp. 1165–1166, Aug. 2002.

[13] G. Fikioris, I. Tastsoglou, G. D. Kolezas, and T. Hatziafratis, "Unphysical moment-method solutions of an approximate integral equation of electrostatics," *IEEE Antennas Propag. Mag.*, vol. 59, no. 3, pp. 142–153, Jun. 2017.

[14] B. Zubik-Kowal and P. J. Davies, "Numerical approximation of time domain electromagnetic scattering from a thin wire," *Numer. Algorithms*, vol. 30, no. 1, pp. 25–36, 2002.

[15] H. Brunner, *Collocation Methods for Volterra Integral and Related Functional Differential Equations*. Cambridge, U.K.: Cambridge Univ. Press, Nov. 2004.

[16] D. S. Jones, "Note on the integral equation for a straight wire antenna," *IEE Proc. H Microw., Opt. Antennas*, vol. 128, no. 2, p. 114, 1981.

[17] L. Lombardi, F. Loreto, F. Ferranti, A. Ruehli, L. Fellow, M. S. Nakhla, L. Fellow, Y. Tao, M. Parise, and G. Antonini, "Time-domain analysis of retarded partial element equivalent circuit models using numerical inversion of Laplace transform," *IEEE Trans. Electromagn. Compat.* early access, Oct. 27, 2020, doi: 10.1109/TEMC.2020.3029448.
[18] G. Flynn, "Numerical methods for improper integrals," *College Math. J.*, vol. 26, no. 4, pp. 284–291, Sep. 1995.

SHUJI KITORA was born in Hyogo, Japan, in 1990. He received the B.S., M.S., and Ph.D. degrees in engineering from Osaka University, Osaka, Japan, in 2015, 2017, and 2021, respectively.

His research interests include EMC and computational electromagnetics.

SOUMA JINNO was born in Ehime, Japan, in 1992. He received the B.S., M.S., and Ph.D. degrees in engineering from the Graduate School of Engineering Science, Osaka University, in 2015, 2017, and 2020, respectively. He has been with the ABE Laboratory as a JSPS Research Fellow, since 2019. His research interest includes electromagnetic noise.

HIROSHI TOKI was born in Osaka, Japan, in 1946. He received the B.S., M.S., and Ph.D. degrees in physics from the Faculty of Science, Osaka University, in 1974.

He stayed in Juelich for three years, from 1974 to 1977, and in Regensburg, Germany, for three years, from 1977 to 1980. From 1980 to 1983, he was an Associate Professor with Michigan State University, East Lansing, MI, USA, for three years. From 1983 to 1993, he was with Tokyo Metropolitan University for ten years. In 2010, he was a Professor with Osaka University until his retirement. His research interests include theoretical nuclear physics, hadron physics, and electric circuit. He was awarded the Humboldt Research Prize, in 2000, and the Japan Physical Society Paper Award, in 1993 and 2011.

MASAYUKI ABE (Member, IEEE) was born in Kobe, Japan. He received the Ph.D. degree in engineering from the Graduate School of Engineering, Osaka University, in 1999. He worked with Toshiba Corporation as an Engineer of storage devices for two years. He was an Associate Professor with Osaka University, from 2003 to 2011, and Nagoya University, from 2012 to 2014. He moved to Osaka University as a Full Professor, in 2014. His research interests include scanning probe microscopy and physics of noise. He was awarded Feynman Prize, in 2009.